Parameter Optimisation

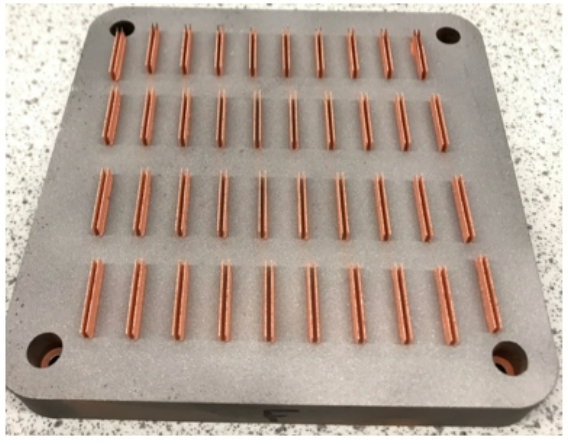

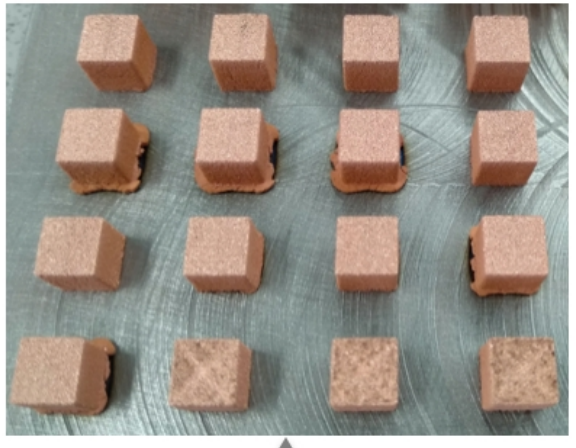

Scan strategies

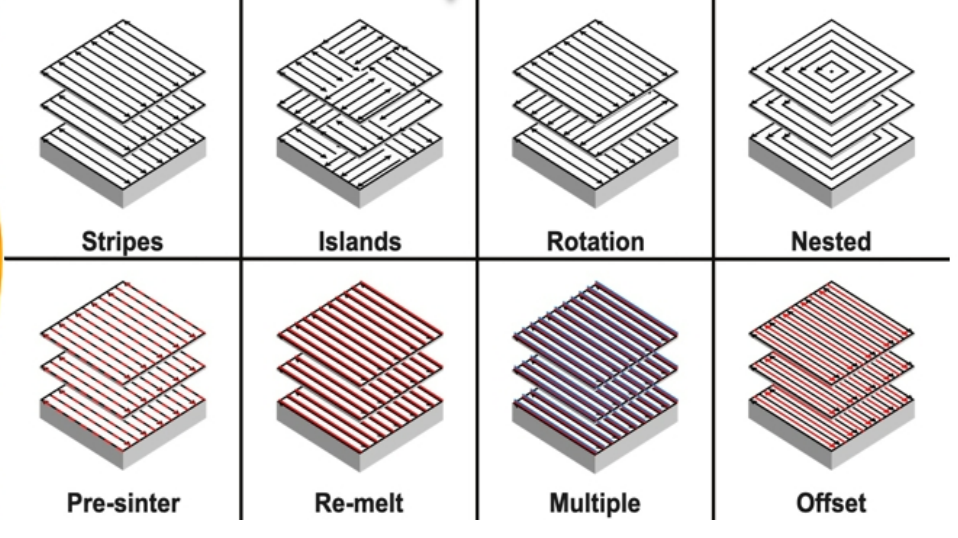

Post Heat Treatment

Decreased Isotropic Resistivity

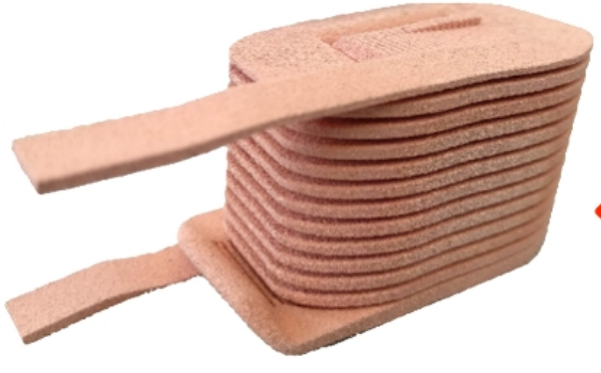

Electrical resistivity of pure copper processed by medium-powered laser powder bed fusion additive manufacturing for use in electromagnetic applications

Cassidy Silbernagel [a??,*,1], Leonidas Gargalis [a??,1], Ian Ashcroft [a], Richard Hague [a], Michael Galea [b,c], Phill Dickens [a]

a Centre for Additive Manufacturing (CfAM), Faculty of Engineering, University of Nottingham, Nottingham NG7 2GW, UK
b Power Electronics, Machines and Control Group, Faculty of Engineering, University of Nottingham, Nottingham NG7 2RD, UK
c School of Aerospace, University of Nottingham Ningbo China, Ningbo 315100, China
** Corresponding author*
1 These authors contributed equally to this work.

Abstract

Pure copper is an excellent thermal and electrical conductor, however, attempts to process it with additive manufacturing (AM) technologies have seen various levels of success. While electron beam melting (EBM) has successfully processed pure copper to high densities, laser powder bed fusion (LPBF) has had difficulties achieving the same results without the use of very high power lasers. This requirement has hampered the exploration of using LPBF with pure copper as most machines are equipped with lasers that have low to medium laser power densities. In this work, experiments were conducted to process pure copper with a 200W LPBF machine with a small laser spot diameter resulting in an above average laser power density in order to maximise density and achieve low electrical resistivity. The effects of initial build orientation and post heat treatment were also investigated to explore their influence on electrical resistivity. It was found that despite issues with high porosity, heat treated specimens had a lower electrical resistivity than other common AM materials such as the aluminium alloy AlSi10Mg. By conducting these tests, it was found that despite having approximately double the resistivity of commercially pure copper, the resistivity was sufficiently low enough to demonstrate the potential to use AM to process copper suitable for electrical applications.

Highlights

- Medium powered LPBF machines can process pure Cu to an acceptable level.
- Resistivity of as-built Cu increases by 33% depending on initial build orientation.
- Resistivity can be reduced by over 50% from as-built conditions via heat treatment.
- Electrical resistivity values once heat treated are lower than AlSi10Mg values.

Keywords

- laser powder bed fusion;
- copper;
- additive manufacturing;
- 3D printing;
- electrical resistivity;
- electrical conductivity;

Introduction

Additive manufacturing (AM) for electromagnetic applications such as electric motors is an area being increasingly studied and researched. Researchers are investigating the use of laser powder bed fusion (LPBF) with soft magnetic materials such as silicon steel[1–3] and hard magnetic materials such as neodymium-based materials [4,5]. However, a major component of all electromagnetic applications is the ability to create a magnetic field through coils or windings of highly conductive metals. LPBF has also been used to explore such materials as silver[6], gold[7], aluminium[8], and the aluminium alloy AlSi10Mg[9]. Copper is widely used in electrical components due to its balance of low electrical resistivity and moderate commodity price compared to gold and silver. However, pure copper has proven challenging to process with most AM technologies. Electron Beam Melting (EBM) has been used to process pure copper with some electrical measurements reported[10,11], however, the method reported does not directly measure resistivity, but rather it back calculates surface conductivity and assumes isotropic properties[12].

Previous attempts of LPBF with pure copper have shown that the process is difficult to control due to the inherent properties of the material. Challenges arise in reaching a density higher than 80-88% [13,14] due to the inability to fully re-melt previously deposited copper with lasers that had an average laser power density of 5-10 MW/cm^2, of which most commercial LPBF machines are in this range. Copper's high thermal conductivity [15] causes rapid heat transfer away from the melt pool through the previously solidified material. Solid copper is also very reflective at the laser wavelengths used in LPBF (~1094 nm), reflecting 90-98% of the incoming thermal energy [16], however, it has been stated that copper powder reflects only 71-72% of the energy, depending on particle size [17]. An unstable melt pool which results in balling [18], due in part to the rapid formation of oxide layers [19]on the melt pool surface, adds to the difficulties in using LPBF to process copper.

To overcome these challenges, researchers have explored a few different options. High power lasers (400 W and 1 kW) have been used [20] to create high-density parts (96.47%), however, no electrical measurements were given. The use of different wavelengths of lasers is also being explored with copper [21] as Cu has a higher absorption to wavelengths less than 532 nm [16]. For example, the Fraunhofer Institute for Laser Technology (ILT), stated that they are investigating the processing of copper via LPBF using a custom built 400-watt green laser (515 nm wavelength) [22]. TRUMPF has also demonstrated the printing of copper with a green laser [23] with a maximum power output of 1 kW[24]. Blue lasers are now being investigated to weld copper with wavelengths of 450 nm [25] and powers up to 700 W [26]. An alternative approach to improving the laser processability of copper is through alloying; however, elemental modification to pure copper generally tends to negatively influence the resistivity of the resultant copper alloy. Specialised alloys such as GRCOP-84 [27,28] which have 8% chromium and 4% niobium have been developed by the NASA Glenn Research Center and work best with rapid solidification technology like LPBF. This is in order to minimise the growth of Cr_2Nb precipitates which give it excellent high-temperature strength and good creep resistance whilst also retaining relatively high thermal and electrical conductivity - close to 70% of the International Annealed Copper Standard (IACS). The IACS compares the resistivity of a material to a commercial standard (1.7241 μΩ-cm equals 100% IACS) [29].

Although many of the investigations into processing copper with LPBF refer to electrical properties, surprisingly few have reported on the actual conductivity or resistivity

achieved. In one of the published works that did report electrical properties, a 300W LPBF machine was used with a copper powder that was first reduced by hydrogen gas to remove oxides, and then coated with a few nanometres of polydimethylsiloxane (PDMS) to inhibit oxidation [30]. The PDMS would then be vaporised in the AM process. Experiments achieved a density of 91%, however, the conductivity was far below expected (maximum 16% IACS) for this density and copper purity (99.4% as stated by the manufacturer). It was found that the copper used in the experiment had 0.6% phosphorus in the starting powder, which has a severe negative effect on conductivity. Others have tested copper alloys with 3.3-5% tin [31,32] which resulted in high-density parts. They performed electrical tests using a 4-point Kelvin measurement system which measured up to 24% IACS as-built and through thermal ageing were able to improve this to 43.2% IACS.

Despite the potential of high porosity, processing pure copper with AM can, in turn, enable printing of coils for electrical machines as long as the conductivity and strength are sufficiently high for such applications. Coils for electrical machines are traditionally hand-made components and today remain a limiting factor on the operation and rating of the machine [33]. The ability to print coils enables a step change in the design and manufacture of these components, where customised and/or modulated turns can be achieved. Another advantage would be the achievement of higher slot fill factors which could increase efficiency and power density. This could reduce the size and weight of electric motors, making them more suitable for aerospace and automotive applications [34]. This work explains the suitability of using an averagely powered (200 W) LPBF system with a small spot size to process copper to the maximum density achievable. Electrical testing using direct 4-point Kelvin measurements was undertaken with respect to initial build orientation. Post heat treatment was carried out to measure the effect on electrical resistivity.

Material and Methods

Powder characterisation and LPBF equipment

A nitrogen gas atomised spherical pure copper powder supplied from ECKA Granules GmbH (Germany), with a minimum 99.9 wt. % copper purity and an apparent density of 4.80 g/cm^3 (ISO3923/1) was used in this work. The average size of the particles was 38.0 µm with 90% of the particles below 65.3 µm, as measured by a Mastersizer 3000 from Malvern Instruments Ltd. (UK). The powder was imaged and analysed using a desktop Hitachi High-Technologies Corp. (Japan) TM3030 scanning electron microscope (SEM) with backscattered electron detection. Images were taken using an acceleration voltage of 15 kV along with an energy dispersive X-ray (EDX) spectrometer for elemental composition analysis. The powder had no trace of interstitial elements as determined through EDX analysis.

A Renishaw plc (UK) AM125 LPBF machine was used to process the copper, which was equipped with a 200-watt D Series redPOWER ytterbium fibre continuous wavelength (CW) laser from SPI Laser (UK) with a near infrared wavelength of 1070 nm (±10 nm) and a spot size of 35 µm (±5µm). This resulted in a laser power density of 20.8 MW/cm^2. The AM125 had a build volume of 125 mm^3 with a base plate heater, set to 170 °C, which was maintained throughout the build process. A vacuum and argon purge was used in the build chamber in order to keep oxygen content below a maximum of 500 parts per million, however actual processing conditions averaged below 300 ppm. Mild steel substrates were used as this has been found to be a suitable material to build copper parts upon as there is good bonding between these two materials [19].

Design of Experiments

The traditional Taguchi approach [35] was implemented to vary and identify the set of process parameters that maximised the density for high purity copper. The implementation of this design of experiments (DOE) assesses the impact of influence factors, such as process and material parameters, on objective factors such as the density and dimensions of single lines and thin walls. These combined process parameters partially control the part quality and the types and number of defects in the parts.

Studies into the formation of single tracks are first necessary to understand the melting and solidification behaviour in the process. This includes the response of the target material towards being irradiated with a laser beam. The stability, irregularity, and discontinuity zones seen in single track experiments help to narrow down the processing parameters, avoiding waste of material and time producing bulk samples at all possible combinations of parameters. These experiments were designed in a systematic procedure based on Taguchi's approach.

After creating the single tracks, they were analysed to study two different properties. First to evaluate the presence of irregularities and distortions along the length of a scan track, i.e. defining zones of continuity. Second to measure the depth and width of each melt pool from the cross-sections of a scan track. Comparison of these two properties at different processing parameters leads to a narrowing down of the process window by finding the most uniform and consolidated scan track. According to Kempen et al. [36], there are some requirements that need to be fulfilled in the formation of single tracks for a successful LPBF process, these are: (1) the deposition of a continuous track, (2) each layer must penetrate the previous layer, (3) each layer has to be high enough to build up the part cumulatively, and (4) the connection angle with the previous layer should be close to 90°.

In order to best evaluate these four requirements, thin walls were then fabricated. These thin walls were also used to study layer thickness, wettability and intralayer bonding. Although layer thickness can partially be determined by measuring the height of single tracks, they don't provide all the necessary information for successfully manufacturing a part. A suitable layer thickness can ensure proper bonding between layers to allow an adequate depth of penetration for the laser scan tracks and provide adequate remelting of the previously deposited areas. Good interlayer bonding can minimize the possibility of interlayer cracking and can reduce pore formation. This bonding is also controlled by wettability, i.e. the melt pool evenly attaching and spreading over the substrate or the previous layer, rather than clumping or balling.

In order to obtain a fully dense part with good dimensional accuracy, studying the geometrical characteristics of the single track has to be ensured and a good bond between each layer and the previous one must be achieved. However, this alone does not ensure a good final part. Thus, cubes were fabricated as the last step of the DOE in an effort to produce high-density copper parts. These cubes were then used to study hatch spacing and the effects of the scan strategies on density.

Processing Parameters

According to the DOE followed for this work, some of the LPBF printing parameters were varied, while others were held constant. This was done in order to find the optimal parameters for maximum density. The variables are found in Table 1.

Table 1: LPBF parameters and the corresponding value or range to be tested.

Parameter	Value or Range
Laser power (W)	200 (maximum available)
Laser spot diameter (µm)	35 (minimum)
Powder bed temperature (°C)	170 (maximum allowable)
Laser scan speed (mm/s)	50 to 1250 (in increments of approx. 25)
Layer thickness (µm)	30, 45, 60
Laser beam focus position (mm)	-10 to 10 (in increments of 1, with increments of 0.2 between -1 and 1)
Hatch spacing (µm)	50 to 175 (in increments of approx. 10)
Scan strategies	Stripes, Islands, Rotation, Pre-sinter, Re-melt, Multiple Scan, Offset Hatch, Nested Contours

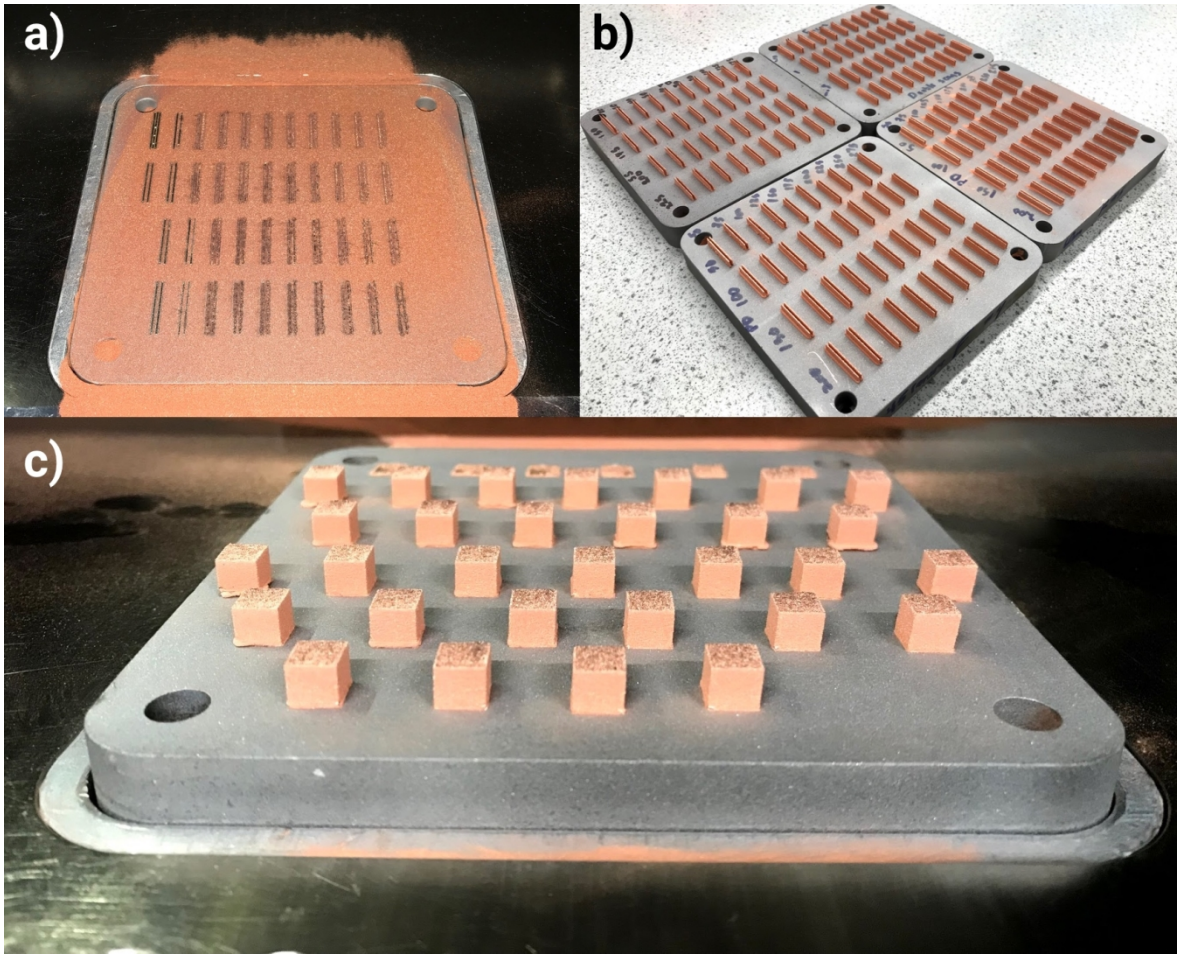

Figure 1: As-built scan tracks a), thin walls b), and cube specimens c) made of pure copper for parameter optimisation.

A pair of single scan tracks which were 18mm long were created for each parameter set tested according to the DOE. The second line for each set had the laser scanning in the opposite directions to the first line. Two tracks per parameter set were made in order to average out variations in processing. These were created to define the processing window for scan speed as seen in Figure 1 a). The speeds for single tracks were limited to those previously reported in the literature, between 50 and 275 mm/s in increments of 25. As laser-scan speed was defined as an exposure time and a point distance, four point distances (50 to 200 in increments of 50) were investigated. Tracks were created on a temporarily bonded thin steel plate that could be removed and sectioned easily.

Next, a pair of thin walls were fabricated for each parameter set of the DOE which were 18 mm long, and 4 mm tall, as shown in Figure 1 b). These were used to evaluate the intralayer bonding with a layer thickness being varied in the range 30-60 μm at intervals of 15μm. Thin walls were also used to evaluate the effect of focus position on quality with tests conducted from -10 mm to 10 mm, at increments of 1 mm, including tests between -1 to 1 at increments of 0.2 mm. Tests on thin walls were also conducted with multiple passes of the laser, with different laser powers (100, 150, and 200 W) in different orders to evaluate their effect on weld track continuity. In order to find the optimal point distance, a wider range of point distances was selected (25 to 175 μm in increments of approximately 25) to be tested at four laser speeds (150, 175, 200, 225 mm/s) at 200 W. Once a point distance was selected, a wider range of laser speeds was investigated, from 200 to 1250 mm/s in increments of approximately 25.

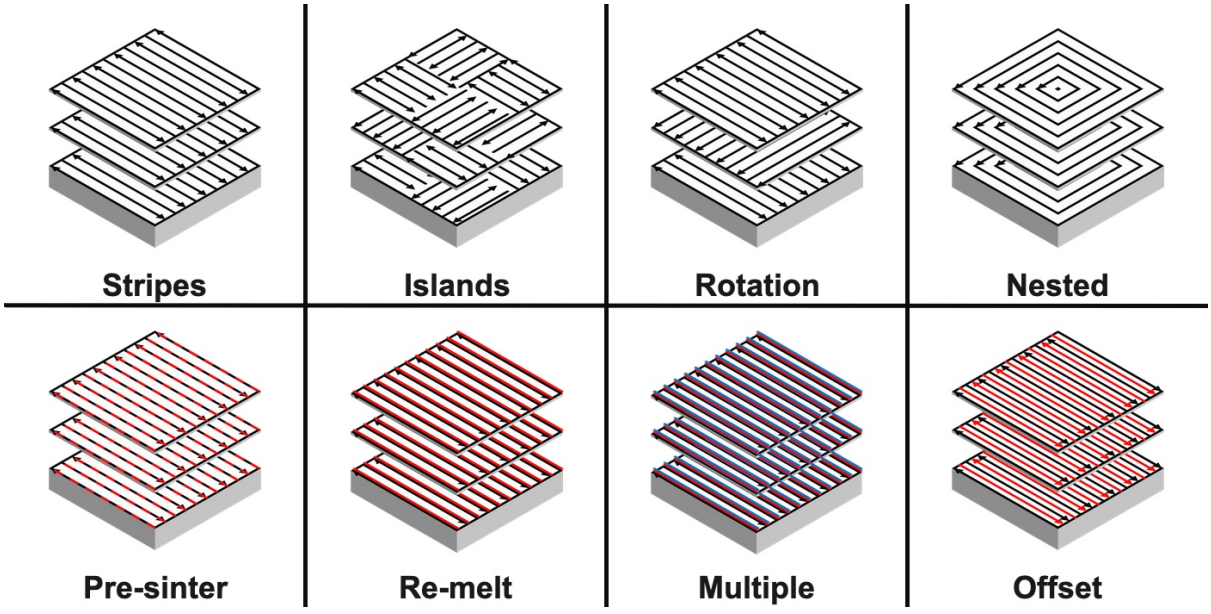

Figure 2: Examples of the scan strategies which were used in the manufacturing of cubes, with single scan strategies along the top and multiple scan strategies along the bottom.

Cubes with an edge length of 5 mm were then fabricated using the best DOE based parameters for layer thickness, focus position, point distance and exposure time as seen in Figure 1 c). Cubes were made to evaluate hatch distance and scan strategies with respect to density and interlayer bonding. The scanning strategies presented in Table 1 are seen in Figure 2 and were used in an attempt to minimise defects and increase the density of the as-built parts. Hatch distances between 50 and 175 μm with increments of approximately 10 were investigated along with both single scan strategies named Stripes, Islands, Rotation, Nested Contours, and multiple scan strategies named Pre-sinter, Re-melt, Multiple, and Offset Hatch, all shown in Figure 2. Cubes were created

first with a stripes scan pattern testing the hatch distance range with respect to cross-sectioned optical density measurements.

Preparation of specimens

Once printed and removed from the baseplate, cubes were encapsulated in a non-pressurized cold mount resin. This was used in preference to a pressurized hot mounting process where the heat and pressure of this sample preparation process could skew density measurements and deform as-built features due to the ductility and anticipated porosity of the processed copper. Specimens were ground flat and polished according to the Struers ApS (Denmark) guide for pure copper. Grain boundaries were identified using a macro etch solution of 50 mL Nitric Acid (1.40 pH) and 50 mL water with a submersion into the solution for 2 seconds followed by a water rinse. Optical Density measurements were made through threshold selection of contrasting areas in the open-source software Fiji [37], as well as on additional cubes which were not resin mounted using the Archimedes principle on a Helium Pycnometer made by Micromeritics (USA), model AccuPyc 1330. Relative densities were initially measured by a single cross-section optical density measurement using thresholding limits. The region of interest for the optical measurements was a square inset from the edge 0.1 mm.

Test bars were designed and printed (nominally 2 mm x 2 mm x 25 mm) so that the expected resistance for each bar would be at least 100 μΩ at 100% IACS in accordance to ASTM B193-02 "Standard Test Method for Resistivity of Electrical Conductor Materials" [29]. Laser-scan parameters for these bars were selected from the set that resulted in the highest density from the DOE test cubes. Three bars were created for each test case. Three initial build orientations (horizontal, 45-degree, vertical) were tested for each test case, where the direction of the longest edge of the bar defined the name of the orientation. Test cases included as-built, two post heat treatment temperatures (800 °C and 1000 °C) and three post heat treatment dwell times (30 minutes, 1 hour, 4 hours). This resulted in the creation of 63 test bars for testing, as seen in Figure 3 along with two test coils. Temperatures for heat treatment represent the range at which copper will sinter [38] before it melts at 1083 °C [39]. Heat treatments were conducted in a tube furnace with an argon inert atmosphere. Test bars were placed in crucibles to avoid any contamination. The ramp up temperature was set at 10 °C per minute for all heat treatments, followed by furnace cooling to room temperature.

Despite the potential for high porosity, in order to further refine the electrical resistivity of pure copper processed by LPBF and to investigate some design elements, two test electrical coils were created as seen in the middle of the build plate of Figure 3. They were manufactured in the same build as the test bars using the same processing parameters as the resistivity test bars and were subjected to a heat treatment at 1000 °C for half an hour. The lack of insulation material in the samples was made up for by the controlled air-gaps between turns, which was another perceived advantage of printing coils and was one of the design elements investigated. The resistivity was measured using the same method as the test bars with a temporary insulation material used to prevent accidental short-circuits between turns. Resistance measurements were taken and were correlated using the CAD wire lengths of 1267 mm and 650 mm respectively and as-built cross-sectional geometries.

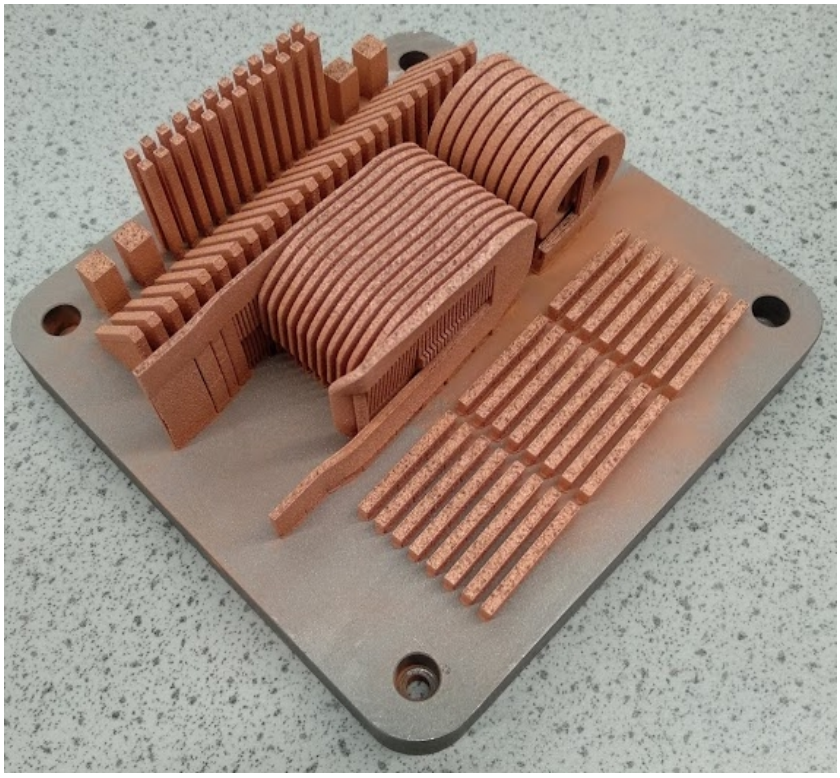

Figure 3: Build plate with electrical test bars manufactured in vertical, horizontal and 45–degree orientation along with prototype coils and test cubes.

Electrical Test Methodology

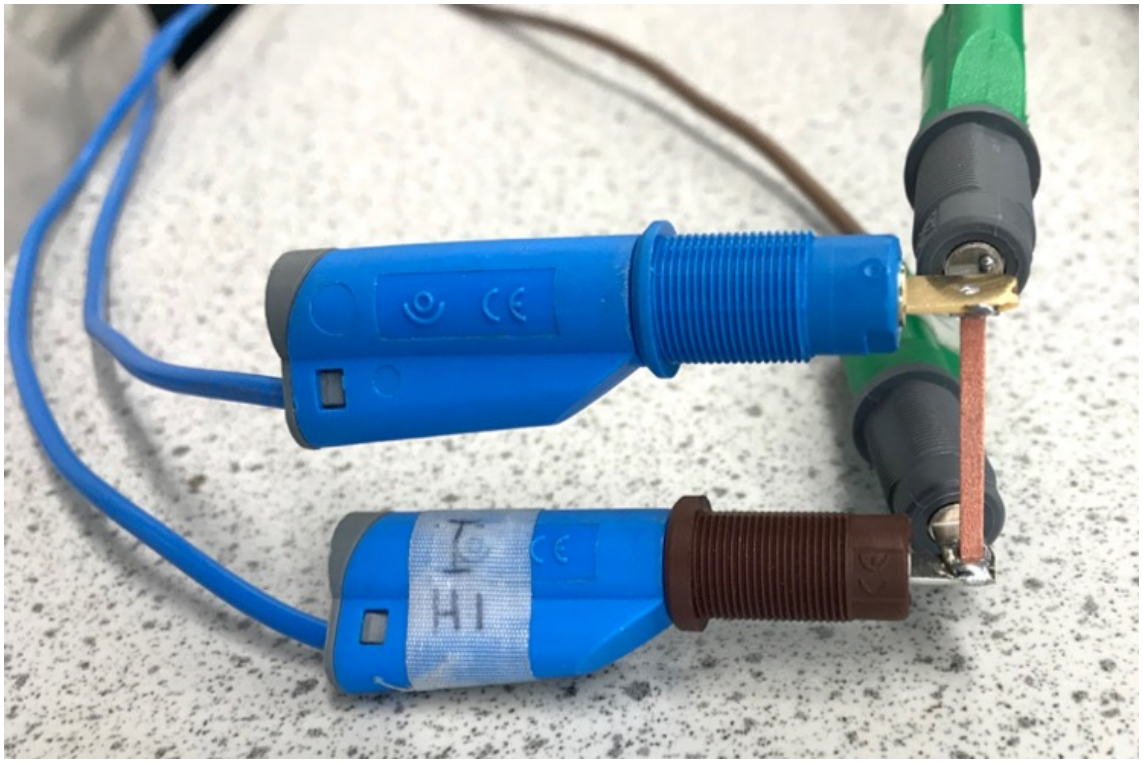

Figure 4: Copper test specimen soldered directly to electrical tabs in order to minimise contact resistance as measured by a 4-point probe.

Electrical DC resistance testing was performed using a Valhalla Scientific Inc. (USA) 4300B digital micro-ohmmeter. This DC four-wire Kelvin resistance measurement meter was calibrated to within 5% accuracy by an external vendor and verified internally through tests using precision low-resistivity resistors and current shunts. It was capable of generating a current between 0.1 mA and 10 A and able to measure the voltage from 20 mV to 2 V, with a minimum sensitivity of 1 μV. After heat treatment and a light hand filing, specimens were individually measured along all dimensions, in a minimum of four places using Mitutoyo digital calipers which had an accuracy of ±0.02 mm. This was undertaken to accurately determine the cross-sectional area and length of each specimen. Electrical tabs were then soldered on in order to minimize contact resistance between the specimen and the voltage probes as seen in Figure 4. Each specimen was measured a total of four times, where two measurements were taken in succession, with the test leads being flipped around in accordance to ASTM B193-02 "Standard Test Method for Resistivity of Electrical Conductor Materials" [29]. Measurements were then averaged with the corresponding standard deviations determined.

Electrical resistivity (ρ) measured in μΩ-cm was calculated by $\rho = RA/L$, where R was the measured resistance in μΩ, A was the measured external cross-sectional area of the specimen measured in cm^2, and L was the length of the specimen in cm. It is important to note that the resistivity measurement takes into consideration the porosity of the specimen, as the cross-sectional area is taken from external dimensions (minus any internal channels for hollow specimens). Resistivity is also a function of temperature, but for this investigation, only room temperature values are reported, as the full temperature dependency of resistivity has been previously reported for copper [40].

Results

Single Scan Tracks

In determining the optimal laser scan speed, initially, the range was set to the speeds previously reported in the literature. While initial observations showed good quality melt tracks, upon cross-sectioning and EDX elemental analysis, it was seen that a considerable amount of iron had transported into the melt pool, as shown in Figure 5 b). While this aided in bonding to the substrate, it alters the melt characteristics and does not provide accurate information on the parameters needed for processing pure copper parts. No cracks or pores were observed in the SEM micrographs of the cross-sectioned melt pools as shown in Figure 5 a), proving that the laser power density was sufficient to melt copper. However, the highly elliptical shape of the melt pool indicated that even though the processing parameters were sufficient to create a continuous weld track, the laser melting process remained in the conduction melting regime. Higher laser power and slow scan speeds would cause an increase in energy density, thus, creating a deeper more stable melt pool through a transition towards keyhole melting [41].

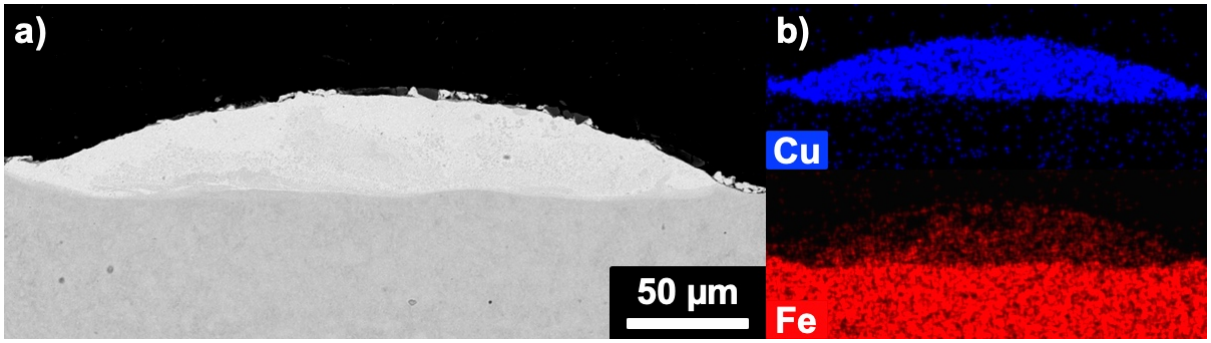

Figure 5: Cross-section of single scan track a), along with EDX analysis for copper and iron content b).

Thin Walls

The same range of laser scan speeds and point distances were used to create thin walls. This test set was repeated for the three different layer thicknesses. As with the single tracks, there was a large amount of iron diffusion into the weld tracks at slower scan speeds. An extreme example can be seen in Figure 6. In this example of a thin wall processed at 50 mm/s, iron had diffused into the melt pool from the bottom of the thin wall for approximately 1.5 mm. Once the copper concentration below the pre-melted powder layer neared 100%, the previously deposited layer with iron failed to re-melt and only pure copper was deposited. This transition from copper-iron to pure copper was characterised by a significant decrease in the wall thickness as seen in Figure 6 b).

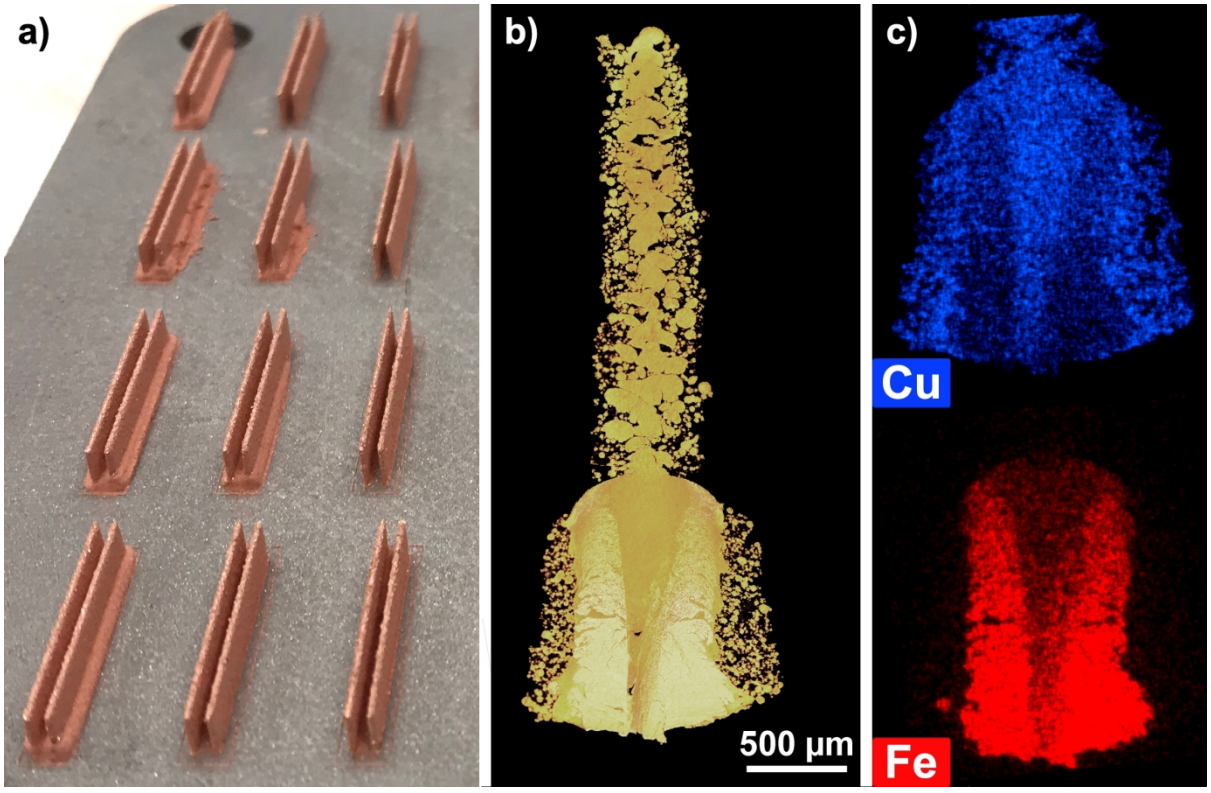

Figure 6: Thin walls in the first column on the left a) were created at a high power and slow scan speeds, a sectioned view b) and EDX analysis c) reveal copper and iron content.

When comparing the results for the three different layer thicknesses, 30 μm layers resulted in some powder spreading issues, which caused the first row of thin walls to have a raised section nearest to the powder re-coater, and random missing portions of the thin wall. The 60 μm thin walls had much less consistent weld tracks with greater amounts of sintering rather than melting. The 45 μm layers showed no signs of powder spreading issues and had much better melting behaviour than the thicker layer. For all remaining tests, a 45 μm layer thickness was used.

The best parameter set from the previous test was chosen to study the effect of the laser beam focus position. Positions below -5 mm showed significant balling, and above 4mm showed increased sintering without any improvements to weld track quality. Between -3 and 3 mm, the tracks showed similar quality with both continuity and width of sintered particles, so the focus position was kept at 0 for all remaining tests.

Use of multiple scans for a single track were investigated as a way to try to improve the density by melting any particles that failed to form part of a continuous weld track. However, neither combinations of the different laser powers nor different orders of those laser powers failed to improve the continuity of the thin walls. Instead, multiple high-power passes only resulted in increased balling in the thin wall.

Next, to find the optimal laser point distance, a wider range of point distances was selected to be tested at four laser speeds at maximum laser power. By comparing these tests along with the first three sets of tests used with different layer thicknesses, it was found that at many different speeds, a 50 μm point distance provided the most consistent thin wall and this was used for the remaining tests.

Finally, a wider range of laser speeds was investigated up to 1250 mm/s. It was expected that the highest laser scan speeds would not sufficiently melt the powder to form a thin wall, however, all parameters successfully resulted in thin walls. However, the fastest scan speeds did result in very thin walls with minimal bonding and low strength. After comparing the continuity of weld-tracks and thickness of the sintered particles, the best resulted from a laser scan speed of 300 mm/s.

Cubes

Cubes were created using the best thin wall DOE results which were a laser power of 200 W, layer height of 45 μm, focus position of 0 mm, point distance of 50 μm and exposure time of 167 μs. Cubes were created first with a stripes scan pattern with an example of a striped scan strategy with no rotation shown in Figure 7. An etched cross-section showing the grain boundaries of a test cube is shown in Figure 8. The average grain size as shown by the etched specimen in Figure 8 varies between 5 and 50 μm, with a mean of around 14 μm.

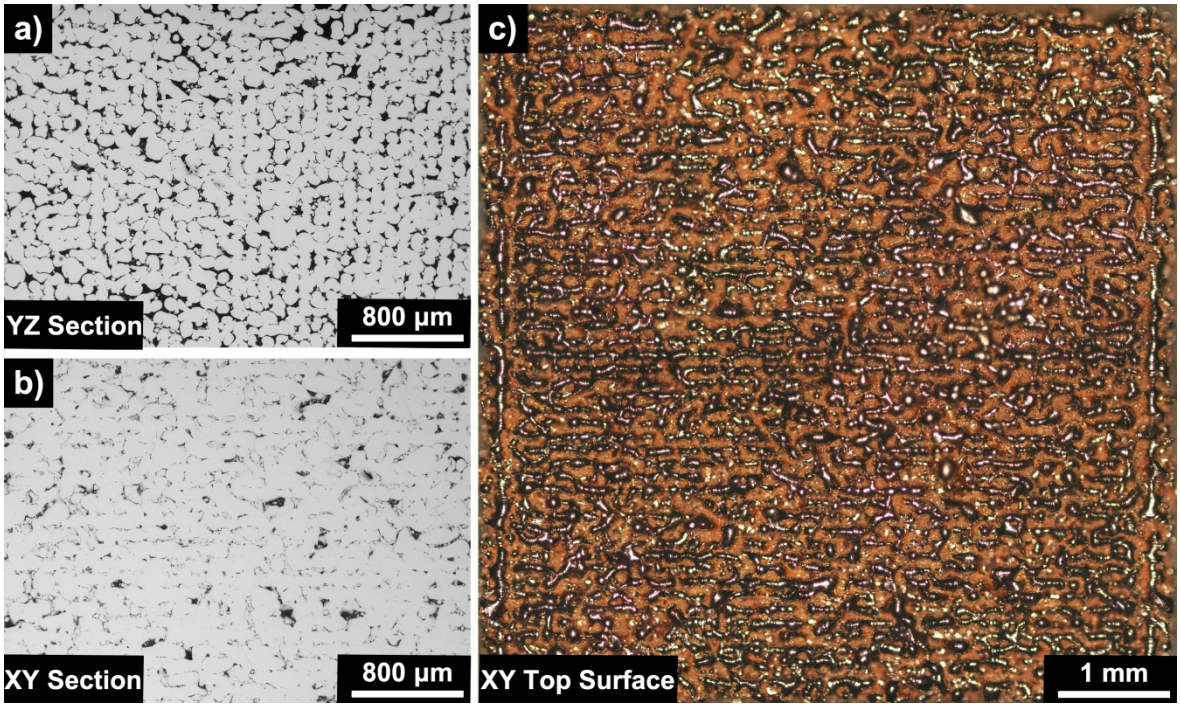

Figure 7: Cross-section of a cube processed with a stripes scan pattern with hatch distance of 100 µm, showing side plane a), top plane b) and an optical image of the top as-built surface c).

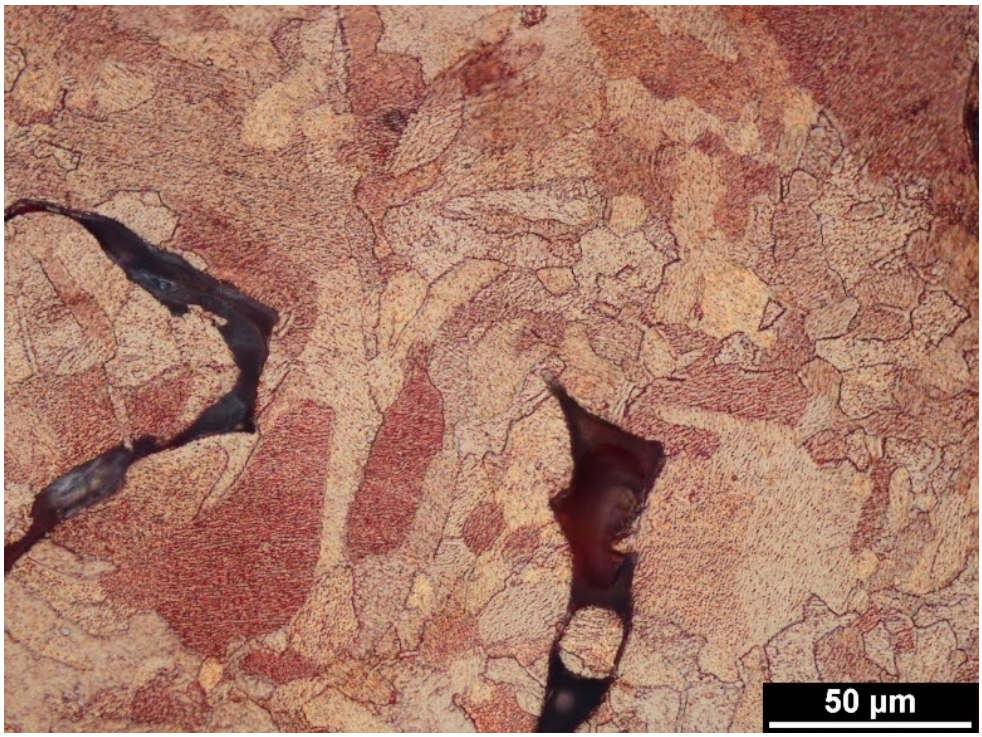

Figure 8: Etched cross-section of XY plane highlighting the grain structure of pure copper processed by LPBF.

After analysing cubes manufactured by the single scan strategies (stripes, islands, rotation, and nested), it was found that there were non-melted areas of loosely sintered powder within and between scan tracks. In an attempt to melt and fuse these areas, multiple scans were applied within a single layer (pre-sinter with lower laser powers, re-

melt by repeating the scan, multiple scans, and an offset scan between tracks). Despite the wide range of tested scan strategies, little change was seen in the corresponding densities. It was found that the multiple scan strategies, whether the second was either directly on top of the previous scan, or offset by half the hatch distance, resulted in 5-15% lower densities than the highest from the single scan strategies. This could be due to a differential in absorptivity between powder and consolidated powder. The highest densities were found with a hatch distance of 100 µm with several of the scan strategies. Rotation of the scan pattern by either 67 or 90-degrees resulted in higher densities compared with non-rotated tests. All single scan patterns with the same scan parameters resulted in densities that were within 5% of each other. After comparing all scan strategies, the final selected set of parameters used a 100 µm hatch distance with a 90-degree rotation each layer.

Density

The highest density using the best scan parameters as measured by optical measurements was 85.8% (± 0.91%). The range of densities for all the different single scan patterns were between 80.3-85.3%, with an average density for all single scan patterns being 83.0%. While an optical single cross-section does not necessarily represent the entire sample, it does provide a good measurement for the corresponding slice from the whole. In order to measure the bulk relative density, a helium pycnometer was also used.

Density measurements using the helium pycnometer were obtained using larger cubes printed in both 90-degree alternating layer scan directions, as well as 67-degrees, as these two patterns were nearly identical in optical densities. Due to the open pores of the test cubes, the resulting densities were approximately 98-99% the density of pure copper. The measured pycnometer volume was then compared to a caliper-measured external volume for a relative density measurement. The average for the 67-degree rotated cubes was 83.5% (± 0.96%) and for the 90-degree cubes was 84.2% (± 1.53%).

Resistivity

The test bars used for resistivity testing were additively manufactured using the cube parameters which resulted in the highest density. This parameter set was a scan strategy of stripes, rotated 90-degrees each layer, and included 3 mm high supports in order to avoid iron contamination. They were printed in a vertical orientation, as well as horizontally and at a 45-degree incline. Some were measured in an as-built condition, while others were subjected to a heat treatment at either 800 or 1000 °C with a dwell time of either 30 minutes, 1 hour, or 4 hours. The resistivity was measured using a DC four-wire Kelvin resistance measurement meter, which directly measured the specimen's resistance. By individually measuring the dimensions of the specimen after heat treatment and a light file of the surface, the material resistivity was determined. The average standard deviation for the length of each specimen was 0.02mm or 0.06% of the length and was 0.01mm for width and height resulting in an average variance in cross-sectional area of 1.1%. The results can be seen in Figure 9. While the average resistivity of the as-built condition specimens was 8.18 µΩ-cm, with heat treatment, the resistivity dropped to the lowest average of 3.69 µΩ-cm for the 1000 °C heat treatment for four hours. The lowest average resistivity for a single initial build orientation was for the 45-degree orientation, heat-treated at 1000 °C for 4 hours, which was 3.43 µΩ-cm which equates to 50.3% IACS. Out of each group of heat treatments, the vertical

orientation had on average 24% higher resistivity than the average of the other two orientations.

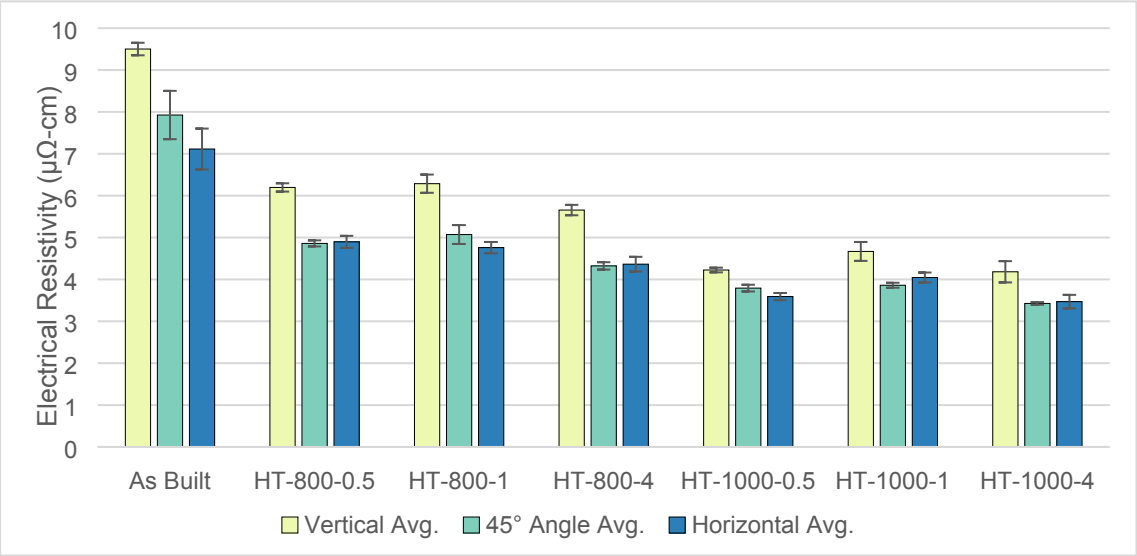

Figure 9: Averaged electrical resistivity of test bars under tested conditions of as-built, heat treatments at either 800 °C or 1000 °C with dwell times of 0.5 hours, 1 hour, and 4 hours with calculated standard deviations.

Demonstration Coils

Two demonstrative electrical coils were created as seen in Figure 10. They used the same processing parameters as the electrical test bars and were subjected to a heat treatment at 1000 °C for half an hour. The resistivity was measured using the same method as the test bars and were correlated using the CAD wire lengths and as-built cross-sectional geometries. Due to the variation between CAD values and the actual external sintered dimensions of the coils, the exact cross-sectional geometry for calculating resistivity was more difficult to estimate. Based on an average of these values for these two coils, the resistivity was determined as 54% IACS which represents the highest conductivity for this study.

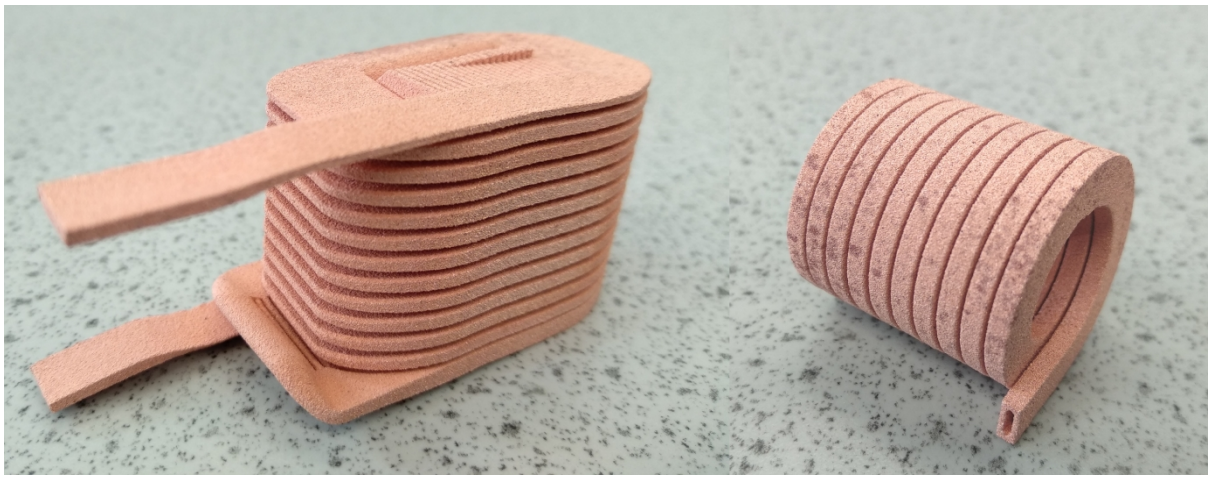

Figure 10: Examples of copper coils created with LPBF showing a variable cross-section (left) and hollow core (right).

Discussion

The electrical resistance of a solid pure metal is derived from the number of disruptions found in the periodic atomic lattice structure [12]. In alloys, this disruption comes from elements that are not the main element of the alloy. However, in pure elements, this disruption comes from imperfections in the crystal lattice. These imperfections are either grain boundaries (seen in Figure 8), vacancies or voids in the atomic lattice, and dislocations in the lattice structure. Larger grains result in lower resistivity due to the lower number of grain boundaries compared to small grain structures. But in the case where the material is not solid but porous, this porosity has the greatest influence on the resistance of the material. Comparing the results in this study to EBM, it can be seen that the LPBF of copper does not create the same columnar grain structures due to a lack of fusion as seen in Figure 8. However, for fully dense high purity copper processed by EBM, the grain boundaries would dominate the resistivity. But due to the use of non-direct eddy-current measurement devices, no anisotropicity was reported in the results in any of the EBM copper studies as eddy-current measurement devices assume isotropic resistivity [12]. This is likely not the true case with EBM due to the columnar grain structure seen in [10,11,42]. The link of an anisotropic grain structure leading to an anisotropic resistivity has been made with LPBF AlSi10Mg [9] and would likely be seen with EBM copper. Thus, for copper LPBF in this study, porosity dominated the resistivity and not grain structure.

In additively manufactured materials, this porosity with respect to resistivity has been studied for a custom aluminium-magnesium alloy and shown to be linear [43]. This linear relationship has also been shown with porous metals manufactured with powder metallurgy methods [44], where the resistivity for copper with a porosity of 15% is approximately 2.5 μΩ-cm or 68.9% IACS. This is better than the best values for samples found in this study, as seen in Figure 9, which is perhaps due to the lack of having a powder compaction pressure in LPBF which is typically used in powder metallurgy methods. The resistivity of highly porous copper can be decreased with further heat treatments at increased temperatures, or through a hot isostatic pressing (HIP) process. The HIP process has been used with additively manufactured copper created using binder jetting [45] where HIP was used after an initial de-binder heat treatment at 450 °C followed by a three-hour dwell at 1075 °C in a hydrogen atmosphere. This HIP and heat treatment process achieved a density of 97.32% (which was aided by a bi-modal powder size distribution), but unfortunately, no resistivity measurements were reported. Heat treatment without HIP have resulted in densities of between 85.5 and 92%, but densities above 92% are needed for HIP because HIP cannot close any surface-connected porosity.

In all tested conditions, the specimens built in a horizontal orientation had the lowest value of electrical resistivity in comparison to the other two orientations, resulting in an anisotropic resistivity. This is reasoned by the cross-section of the top plane (XY) in Figure 7 b) which shows more continuous tracks and fewer discontinuities than in the side plane (YZ) seen in Figure 7 a). The weld tracks in-plane can be thought of as poorly connected wires travelling horizontally. The highest resistivities were found in the vertically built specimens regardless of the applied heat treatments. This is due to an accumulation of partially melted tracks in the build direction (z-axis), in addition to the interlayer and intralayer defects such as incomplete fusion holes and pores due to the unstable melt pool [46]. These accumulations can be thought of as layers of poorly connected thin sheets, which have a higher resistance than the in-plane poorly connected wires. These defects and lack of interlayer fusion reduced the amount of

connected material in the direction of current flow in electrical testing which resulted in a higher electrical resistivity for the vertically built specimens.

In comparing the as-built condition to the most intense heat treatment, the vertical specimen was fractured and analysed using SEM as seen in Figure 11, with the as-built samples on the left and the sample heat treated at 1000 °C for 4 hours on the right. As seen, in the as-built condition there are a number of un-melted powder particles in between the laser weld tracks. There are also noticeable defined edges between tracks. comparing this to the heat -treated case, while there are still some attached powder particles, they appear to not be loose between the tracks but rather fused to them. The number of smaller un-melted powder particles was also reduced after the heat treatment, to indicate sintering or partial melting. The weld tracks also appear to be fused together and do not show the same defined edges between them. This heat treatment effectively sintered the as-built components and caused necking to occur for both the un-melted powders and for tracks that were adjacent to each other. This necking can be seen in Figure 12 where a number of fracture surfaces are identified. This necking and partial sintering decreased the number of discontinuities and gaps in the copper, minimizing the effective path length electricity has to travel, and thus reducing the resistivity of the specimen. Signs of oxidation (as indicated by EDX) were seen as small spots in some areas of specimens but were not measured as the goal of this study was to find the trends of electrical properties with respect to orientation and heat treatment with this class of machine. Further studies with machines better suited to process copper to a higher density should have an oxygen threshold lower than 500 ppm in order to maximise conductivity.

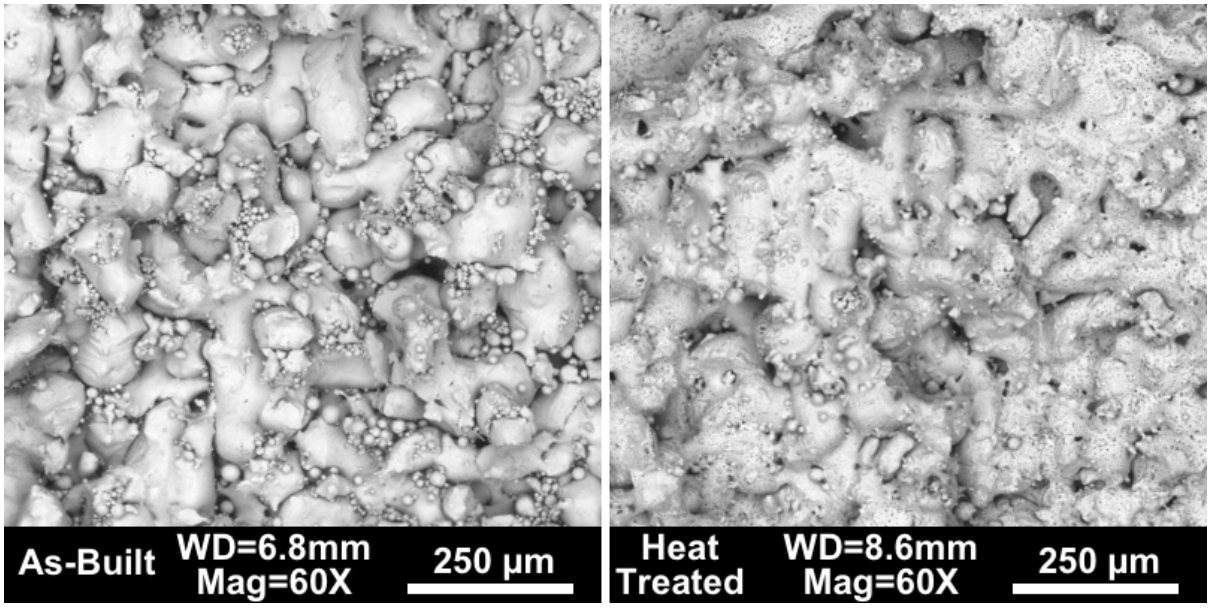

Figure 11: Comparison of a fractured section showing many layers of the (left) as-built vertical test bar and (right) heat treated at 1000℃ for 4 hours vertical test bar.

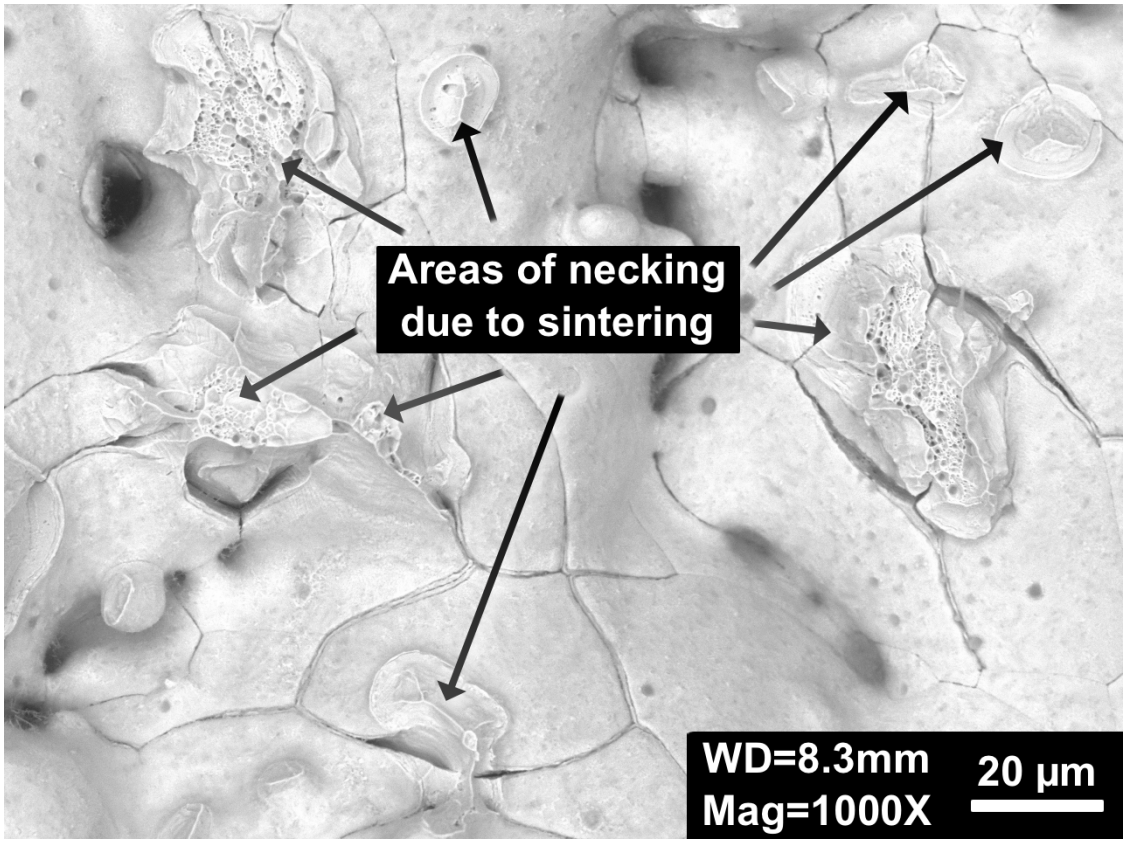

Figure 12: Areas on the fracture surface where localised necking of particles and weld tracks occurred but were broken off.

In order to minimize contact resistance in comparison to the actual material resistance, the ends of the test bars were soldered to the electrical tabs used for testing. However, this soldering could cause some of the variations seen in the measured resistivity values as, due to having a liquid phase metal on a porous surface, some wicking of solder into the ends of the test bars can occur. Whilst this can help reduce porosity, the resistivity of solder is much higher than copper at 15 µΩ-cm being composed of 50% tin and 50% lead. Additionally, some variations in resistivity can be attributed to small differences in porosity (2-4%) between specimens due to the unstable build process. This wicking of the solder into the ends was confirmed by using EDX on a sectioned specimen as seen in Figure 13. Multiple specimens were sectioned to investigate this effect and it was observed that the solder wicked an average of 0.6 mm into the test surface. If the solder completely filled all the voids in this section, it would have a resistance of 3.8 µΩ which corresponds to between 0.9-1.95% of the resistance of the specimens.

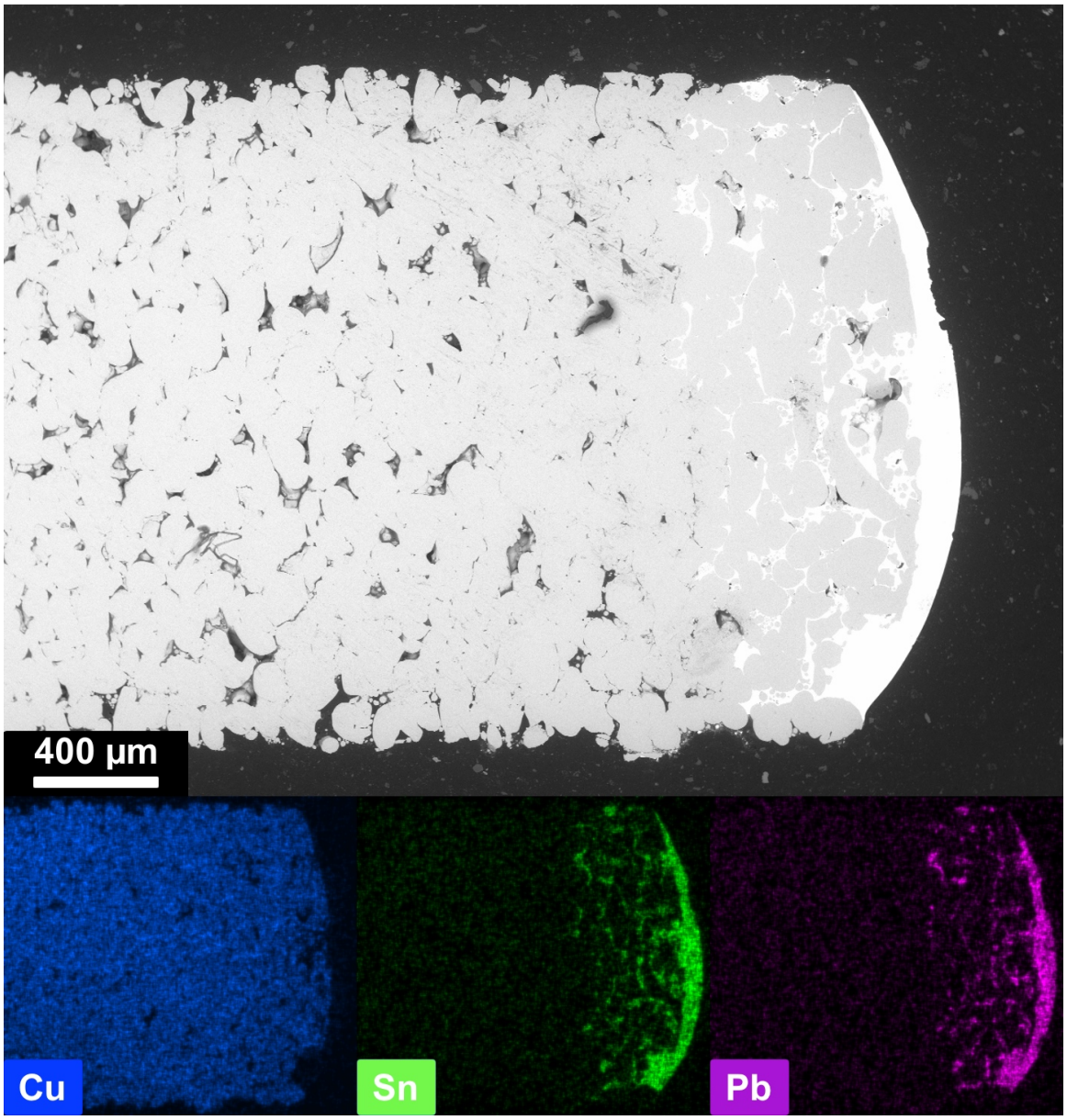

Figure 13: Sectioned SEM image of the soldered end of a copper test bar (top), along with EDX elemental analysis (bottom) showing copper, tin and lead.

Based on the results from this study, the resistivity of pure copper can be compared to the resistivity of other materials processed by LPBF. Despite having relatively high porosity, pure copper proves to be the best material choice in comparison to other metals and alloys processed with a 200W LPBF machine, in terms of conductivity. The best value from the bar specimens achieved was 50.3% IACS. This was better than AlSi10Mg at 30.4% IACS [9] and copper-tin alloys at 43.2% [31].

The results represented here indicate that using a 200 W 1070 nm wavelength laser equipped LPBF machine, even with a small laser spot size of 35 µm, cannot provide the energy needed to fully re-melt previous layers of copper. While it can melt the top layer of powder, it cannot completely fuse this newly melted powder to the solid layer below. This is due to the fact that the copper powder absorbs more of the incoming thermal energy from the laser compared to the solid layer. The powder retains more heat as it's unable to conduct this heat efficiently away to other powder particles, whereas the solid layers can conduct the heat away into the surrounding solid parts. By reducing the

thermal gradient between the melt pool and the previously deposited layers, medium powered LPBF machines could potentially process copper more efficiently. This reduction in the temperature gradient requires a higher baseplate temperature, but most researchers already use the highest temperature allowed on the equipment. Even higher power lasers (1 kW) with small spot sizes (40 μm) processing pure copper run the risk of damaging the scanning mirrors due to its high reflectivity as seen in [47]. In order to overcome the challenges of pure copper's high thermal conductivity and high reflectivity, EBM processes or potentially green and blue laser equipped LBPF machines appear to be the best solutions.

As has been widely reported elsewhere, the design freedom of AM allows for structures that cannot be created using traditional methods. In the case of Cu coils, these include varying the cross-sectional shape of a coil while maintaining the cross-sectional area in order to improve the cooling ability of end turn windings or to control local resistances within a coil, as seen in the left of Figure 10. Hollow shapes can also be made for applications which require additional cooling by running either air or a cooling liquid through the centre of the cross-section, as long as the resulting parts are non-porous, as seen in the right of Figure 10. These design elements and this design freedom, along with the ability to print low resistivity materials, can greatly aid in the development of new electromechanical applications.

Conclusions

In this study, pure copper was additively manufactured using a medium powered 200W laser powder bed fusion machine with a small laser spot diameter of 35 μm. Through parameter optimisation, an optimal set of variables was chosen for processing pure copper. This parameter set had a layer thickness of 45 μm, a laser power of 200 W and a spot size of 35 μm with a laser scan speed of 300 mm/s resulting from a point distance of 50 μm and exposure time of 167 μs. Laser beam focus position, hatch distance variation as well as numerous scan strategies failed to improve the laser weld track quality or density of the additively manufactured specimens. The highest density measured was 85.8% obtained through optical measurement techniques. Test specimens were manufactured in either a vertical, 45-degree or horizontal orientation and were either left in an as-built condition or subjected to different heat treatments. Electrical resistivity measurements were taken and showed a correlation between the initial build orientation and the resulting resistivity, with horizontal and 45-degree builds exhibiting the lowest resistivity.

Differences in resistivity between the different orientations were caused by variations in the different interlayer and intralayer defects caused mainly due to lack of fusion and un-melted powder particles. It was found that the heat-treated specimens exhibited lower resistivity than the as-built condition, with the resistivity of the vertically built specimens being 24% higher than the average for the other two orientations. The lowest average resistivity for a single initial build orientation was achieved using a 1000 °C heat treatment for four hours resulting in a resistivity of 3.43 μΩ-cm (50.3% IACS).

Despite the relatively high porosity, the processed copper has a lower resistivity than most commonly processed LPBF materials such as AlSi10Mg (29% IACS). AM allows the design freedom to create structures which are not possible with traditional manufacturing. As a demonstration, electrical coils with variable cross-section shapes and hollow centres were manufactured and heat treated and found to have a resistivity of 3.19 μΩ-cm (54% IACS). The results show that this is a potential material to use

electrically such as in electric motors, novel antenna designs, or in other electromagnetic applications.

Acknowledgements

The authors would like to acknowledge the support received from the technicians of the Centre for Additive Manufacturing (CfAM, University of Nottingham, UK) Mark East, Mark Hardy and Joe White, and Richard Selo for his work in etching specimens. This research was funded by the INNOVATIVE doctoral programme. The INNOVATIVE programme is partially funded by the Marie Curie Initial Training Networks (ITN) action (project number 665468) and partially by the Institute for Aerospace Technology (IAT) at the University of Nottingham.

References

[1] M. Garibaldi, I. Ashcroft, M. Simonelli, R. Hague, Metallurgy of high-silicon steel parts produced using selective laser melting, Acta Mater. 110 (2016) 207–216. doi:10.1016/j.actamat.2016.03.037.

[2] M. Garibaldi, I. Ashcroft, N. Hillier, S.A.C. Harmon, R. Hague, Relationship between laser energy input, microstructures and magnetic properties of selective laser melted Fe-6.9%wt Si soft magnets, Mater. Charact. 143 (2018) 144–151. doi:10.1016/j.matchar.2018.01.016.

[3] A. Krings, A. Boglietti, A. Cavagnino, S. Sprague, Soft Magnetic Material Status and Trends in Electric Machines, IEEE Trans. Ind. Electron. 64 (2017) 2405–2414. doi:10.1109/TIE.2016.2613844.

[4] N. Urban, A. Meyer, S. Kreitlein, F. Leicht, J. Franke, Efficient near net-shape production of high energy rare earth magnets by laser beam melting, Appl. Mech. Mater. 871 (2017) 137–144. doi:10.4028/www.scientific.net/amm.871.137.

[5] J. Jaćimović, F. Binda, L.G. Herrmann, F. Greuter, J. Genta, M. Calvo, T. Tomše, R.A. Simon, Net Shape 3D Printed NdFeB Permanent Magnet, Adv. Eng. Mater. 19 (2017) 1700098. doi:10.1002/adem.201700098.

[6] A. Gebhardt, M. Fateri, J.-S.J.-S. Hötter, M. Knothe, F.M. Schmidt, H. Rieper, A. Gebhardt, J.-S.J.-S. Hötter, M. Knothe, F.M. Schmidt, H. Rieper, Numerical and experimental investigation of selective laser melting of silver, in: Fraunhofer Direct Digit. Manuf. Conf. (DDMC 2012), Berlin, Germany, 2012. https://www.researchgate.net/publication/264548342.

[7] M. Khan, P.M. Dickens, Selective laser melting (SLM) of pure gold, Gold Bull. 43 (2010) 114–121. doi:10.1007/bf03214976.

[8] E. Louvis, P. Fox, C.J. Sutcliffe, Selective laser melting of aluminium components, J. Mater. Process. Technol. 211 (2011) 275–284. doi:10.1016/j.jmatprotec.2010.09.019.

[9] C. Silbernagel, I. Ashcroft, P. Dickens, M. Galea, Electrical resistivity of additively manufactured AlSi10Mg for use in electric motors, Addit. Manuf. 21 (2018) 395–403. doi:10.1016/j.addma.2018.03.027.

[10] P. Frigola, O.A. Harrysson, T.J. Horn, H.A. West, R.L. Aman, J.M. Rigsbee, D.A. Ramirez, F. Medina, R.B. Wicker, E. Rodriguez, L.E. Murr, F. Medina, R.B. Wicker, E. Rodriguez, Fabricating copper components with electron beam melting, Adv. Mater. Process. 172 (2014) 20–24. https://www.asminternational.org/c/portal/pdf/download?articleId=19739462&groupId=10192.

[11] S.J. Raab, R. Guschlbauer, M.A. Lodes, C. Körner, Thermal and electrical conductivity of 99.9% pure copper processed via selective electron beam melting, Adv. Eng. Mater. 18 (2016) 1661–1666. doi:10.1002/adem.201600078.

[12] G.T. Dyos, The Handbook of Electrical Resistivity: New Materials and Pressure Effects, The Institution of Engineering and Technology, London, 2012. doi:10.1049/pbed013e.

[13] P.A. Lykov, E.V. Safonov, A.M. Akhmedianov, Selective laser melting of copper, Mater. Sci. Forum. 843 (2016) 284–288. doi:10.4028/www.scientific.net/msf.843.284.

[14] T.-T.T.T. Ikeshoji, K. Nakamura, M. Yonehara, K. Imai, H. Kyogoku, Selective laser melting of copper, JOM. (2017) 3–7. doi:10.1007/s11837-017-2695-x.

[15] D. Becker, W. Meiners, K. Wissenbach, Additive manufacturing of copper alloys by selective laser melting, in: WLT – German Scientific Laser Societey (Ed.), Proc. 5th Int. WLT-Conference Lasers Manuf., Munich, Germany, 2009: pp. 195–200. https://www.worldcat.org/title/laser-in-manufacturing-2009-proceedings-of-the-fifth-international-wlt-conference-lasers-in-manufacturing-lim-2009-munich-germany-june-15th-18th-2009/oclc/501976029.

[16] J.P. Kruth, X. Wang, T. Laoui, L. Froyen, Lasers and materials in selective laser sintering, Assem. Autom. 23 (2003) 357–371. doi:10.1108/01445150310698652.

[17] M. Khan, Selective laser melting (SLM) of gold (Au), Loughborough University, 2010. https://dspace.lboro.ac.uk/2134/6163.

[18] J.B. Jones, D.I. Wimpenny, R. Chudasama, G.J. Gibbons, Printed circuit boards by selective deposition and processing, in: Proc. 22nd Solid Free. Fabr. Symp., Austin, Texas, USA, 2011: pp. 639–656. http://sffsymposium.engr.utexas.edu/Manuscripts/2011/2011-50-Jones.pdf.

[19] S.R.R. Pogson, P. Fox, C.J.J. Sutcliffe, W. O'Neill, The production of copper parts using DMLR, Rapid Prototyp. J. 9 (2003) 334–343. doi:10.1108/13552540310502239.

[20] D. Zhang, Z. Liu, C. Chua, Investigation on forming process of copper alloys via selective laser melting, in: High Value Manuf. Adv. Res. Virtual Rapid Prototyp., CRC Press, 2013: pp. 285–289. http://www.crcnetbase.com/doi/abs/10.1201/b15961-53.

[21] L. Kaden, B. Seyfarth, T. Ullsperger, G. Matthäus, S. Nolte, Selective laser melting of copper using ultrashort laser pulses at different wavelengths, in: H. Helvajian, A. Piqué, B. Gu (Eds.), Proc. SPIE - Laser 3D Manuf. V, SPIE, 2018: p. 41. doi:10.1117/12.2289959.

[22] Fraunhofer launches "SLM in green" project for 3D printed copper, (2017). https://www.ilt.fraunhofer.de/en/press/press-releases/press-release-2017/press-release-2017-08-30.html (accessed August 31, 2017).

[23] R. Hönl, World premiere at Formnext: green laser from TRUMPF prints copper and gold, TRUMPF Glob. Press Release. (2018). https://www.trumpf.com/en_INT/company/press/global-press-releases/press-release-detail-page/release/world-premiere-at-formnext-green-laser-from-trumpf-prints-copper-and-gold/.

[24] E. Kaiser, E. Dold, A. Killi, S. Zaske, Application benefits of welding copper with a 1 kW , 515 nm continuous wave laser, in: Ind. Contrib. to 10th CIRP Conf. Photonic Technol. (LANE 2018), Fürth, Germany, 2018. https://www.lane-conference.org/app/download/12333125349/11162_LANE2018_Kaiser.pdf.

[25] J.-M. Pelaprat, M. Finuf, R. Fritz, M. Zediker, Seeing things in a new light: High power blue lasers for metal processing, Laser Tech. J. 15 (2018) 39–41. doi:10.1002/latj.201800028.

[26] A. Balck, M. Baumann, J. Malchus, S. Marfels, U. Witte, D. Dinakaran, S. Ocylok, M. Weinbach, C. Bachert, A. Kösters, V. Krause, A. Lell, H. König, B. Stojetz, U. Strauss, A. Löffler, R. V Chacko, 700 W blue fiber-coupled diode-laser emitting at 450 nm, in: M.S. Zediker (Ed.), Proc. SPIE - High-Power Diode Laser Technol. XVI, SPIE, San Francisco, California, USA, 2018: p. 2. doi:10.1117/12.2286631.

[27] D.L. Ellis, D.J. Keller, Thermophysical properties of GRCop-84, Cleveland, Ohio, USA, 2000. https://ntrs.nasa.gov/search.jsp?R=20000064095.

[28] D.L. Ellis, GRCop-84 : A High-Temperature Copper Alloy for High-Heat-Flux Applications, Cleveland, Ohio, USA, 2005. https://ntrs.nasa.gov/search.jsp?R=20050123582.

[29] T.L. Wire, E. Conductors, I. Tem-, ASTM B193-02(2014), Standard test method for resistivity of electrical conductor materials, ASTM International, West Conshohocken, Pennsylvania, USA, 2014. doi:10.1520/b0193.

[30] T. El-Wardany, Y. She, V. Jagdale, J.K. Garofano, J. Liou, W. Schmidt, Challenges in 3D printing of high conductivity copper, in: ASME 2017 Int. Tech. Conf. Exhib. Packag. Integr. Electron. Photonic Microsystems, ASME, San Francisco, California, USA, 2017. doi:10.1115/ipack2017-74306.

[31] A.P. Ventura, C.J. Marvel, G. Pawlikowski, M. Bayes, M. Watanabe, R.P. Vinci, W.Z. Misiolek, The Effect of Aging on the Microstructure of Selective Laser Melted Cu-Ni-Si, Metall. Mater. Trans. A. 48 (2017) 6070–6082. doi:10.1007/s11661-017-4363-8.

[32] A.P. Ventura, C.A. Wade, G. Pawlikowski, M. Bayes, M. Watanabe, W.Z. Misiolek, Mechanical properties and microstructural characterization of Cu-4.3 pct Sn fabricated by selective laser melting, Metall. Mater. Trans. A. 48 (2017) 178–187. doi:10.1007/s11661-016-3779-x.

[33] M. Galea, C. Gerada, T. Raminosoa, P. Wheeler, A thermal improvement technique for the phase windings of electrical machines, IEEE Trans. Ind. Appl. 48 (2012) 79–87. doi:10.1109/tia.2011.2175470.

[34] V. Madonna, P. Giangrande, M. Galea, Electrical power generation in aircraft: Review, challenges, and opportunities, IEEE Trans. Transp. Electrif. 4 (2018) 646–659. doi:10.1109/tte.2018.2834142.

[35] J. Sun, Y. Yang, D. Wang, Parametric optimization of selective laser melting for forming Ti6Al4V samples by Taguchi method, Opt. Laser Technol. 49 (2013) 118–124. doi:10.1016/j.optlastec.2012.12.002.

[36] K. Kempen, L. Thijs, J. Van Humbeeck, J.-P. Kruth, Processing AlSi10Mg by selective laser melting: parameter optimisation and material characterisation, Mater. Sci. Technol. 31 (2015) 917–923. doi:10.1179/1743284714Y.0000000702.

[37] J. Schindelin, I. Arganda-Carreras, E. Frise, V. Kaynig, M. Longair, T. Pietzsch, S. Preibisch, C. Rueden, S. Saalfeld, B. Schmid, J.-Y. Tinevez, D.J. White, V. Hartenstein, K. Eliceiri, P. Tomancak, A. Cardona, Fiji: An open-source platform for biological-image analysis, Nat. Methods. 9 (2012) 676–682. doi:10.1038/nmeth.2019.

[38] R.I. Cable, T.K. Gupta, Intermediate stage sintering, in: G.C. Kuczynski, N.A. Hooton, C.F. Gibbon (Eds.), Proc. Int. Conf. Sinter. Relat. Phenom. 1965 Held Univ. Notre Dame, Gordon and Breach Science Publishers, New York, New York,

USA, 1967: p. 894. https://www.copper.org/resources/properties/129_6/consolidation.html#a2.

[39] J.R. Davis, Copper and Copper Alloys, ASM International, Materials Park, Ohio, USA, 2001. http://www.worldcat.org/title/copper-and-copper-alloys/oclc/46812085&referer=brief_results.

[40] R.A. Matula, Electrical resistivity of copper, gold, palladium, and silver, J. Phys. Chem. Ref. Data. 8 (1979) 1147–1298. doi:10.1063/1.555614.

[41] W.E. King, H.D. Barth, V.M. Castillo, G.F. Gallegos, J.W. Gibbs, D.E. Hahn, C. Kamath, A.M. Rubenchik, Observation of keyhole-mode laser melting in laser powder-bed fusion additive manufacturing, J. Mater. Process. Technol. 214 (2014) 2915–2925. doi:10.1016/j.jmatprotec.2014.06.005.

[42] R. Guschlbauer, S. Momeni, F. Osmanlic, C. Körner, Process development of 99.95% pure copper processed via selective electron beam melting and its mechanical and physical properties, Mater. Charact. 143 (2018) 163–170. doi:10.1016/j.matchar.2018.04.009.

[43] Y. Shi, P. Rometsch, K. Yang, F. Palm, X. Wu, Characterisation of a novel Sc and Zr modified Al–Mg alloy fabricated by selective laser melting, Mater. Lett. 196 (2017) 347–350. doi:10.1016/j.matlet.2017.03.089.

[44] P. Grootenhuis, R.W. Powell, R.P. Tye, Thermal and electrical conductivity of porous metals made by powder metallurgy methods, Proc. Phys. Soc. Sect. B. 65 (1952) 502–511. doi:10.1088/0370-1301/65/7/305.

[45] A. Yegyan Kumar, Y. Bai, A. Eklund, C.B. Williams, The effects of hot isostatic pressing on parts fabricated by binder jetting additive manufacturing, Addit. Manuf. 24 (2018) 115–124. doi:10.1016/j.addma.2018.09.021.

[46] B. Zhang, Y. Li, Q. Bai, Defect formation mechanisms in selective laser melting: A review, Chinese J. Mech. Eng. 30 (2017) 515–527. doi:10.1007/s10033-017-0121-5.

[47] S.D. Jadhav, S. Dadbakhsh, L. Goossens, J.-P. Kruth, J. Van Humbeeck, K. Vanmeensel, Influence of selective laser melting process parameters on texture evolution in pure copper, J. Mater. Process. Technol. 270 (2019) 47–58. doi:10.1016/j.jmatprotec.2019.02.022.